




ELK3 modulates the antitumor efficacy of natural killer cells against triple negative breast cancer by regulating mitochondrial dynamics

Joo Dong Park ¹, Kwang-Soo Kim,² Seung Hee Choi ¹, Gae Hoon Jo,¹ Jin-Ho Choi,¹ Si-Won Park,¹ Eun-Su Ko,¹ Minwook Lee,¹ Dae-Keum Lee,¹ Hye Jung Jang,¹ Sohyun Hwang,¹ Hae-Yun Jung,¹ Kyung-Soon Park ¹

To cite: Park JD, Kim K-S, Choi SH, *et al.* ELK3 modulates the antitumor efficacy of natural killer cells against triple negative breast cancer by regulating mitochondrial dynamics. *Journal for ImmunoTherapy of Cancer* 2022;**10**:e004825. doi:10.1136/jitc-2022-004825

► Additional supplemental material is published online only. To view, please visit the journal online (<http://dx.doi.org/10.1136/jitc-2022-004825>).

Accepted 27 June 2022



© Author(s) (or their employer(s)) 2022. Re-use permitted under CC BY-NC. No commercial re-use. See rights and permissions. Published by BMJ.

¹Department of Biomedical Science, CHA University, Seongnam-si, Korea (the Republic of)

²Department of Neurosurgery, Lou and Jean Malnati Brain Tumor Institute, Robert H Lurie Comprehensive Cancer Center, Northwestern University Feinberg School of Medicine, Chicago, Illinois, USA

Correspondence to

Professor Kyung-Soon Park; kspark@cha.ac.kr

ABSTRACT

Background Triple negative breast cancer (TNBC) is the most lethal subtype of breast cancer due to its aggressive behavior and frequent development of resistance to chemotherapy. Although natural killer (NK) cell-based immunotherapy is a promising strategy for overcoming barriers to cancer treatment, the therapeutic efficacy of NK cells against TNBC is below expectations. E26 transformation-specific transcription factor ELK3 (ELK3) is highly expressed in TNBCs and functions as a master regulator of the epithelial-mesenchymal transition.

Methods Two representative human TNBC cell lines, MDA-MB231 and Hs578T, were exposed to ELK3-targeting shRNA or an ELK3-expressing plasmid to modulate ELK3 expression. The downstream target genes of ELK3 were identified using a combined approach comprising gene expression profiling and molecular analysis. The role of ELK3 in determining the immunosensitivity of TNBC to NK cells was investigated in terms of mitochondrial fission–fusion transition and reactive oxygen species concentration both in vitro and in vivo.

Results ELK3-dependent mitochondrial fission–fusion status was linked to the mitochondrial superoxide concentration in TNBCs and was a main determinant of NK cell-mediated immune responses. We identified mitochondrial dynamics proteins of 51 (Mid51), a major mediator of mitochondrial fission, as a direct downstream target of ELK3 in TNBCs. Also, we demonstrated that expression of ELK3 correlated inversely with that of Mid51, and that the ELK3–Mid51 axis is associated directly with the status of mitochondrial dynamics. METABRIC analysis revealed that the ELK3–Mid51 axis has a direct effect on the immune score and survival of patients with TNBC.

Conclusions Taken together, the data suggest that NK cell responses to TNBC are linked directly to ELK3 expression levels, shedding new light on strategies to improve the efficacy of NK cell-based immunotherapy of TNBC.

BACKGROUND

The clinical success of autologous chimeric antigen receptor (CAR) T cells in patients with lymphoma and leukemia has raised considerable interest in the use of immune cells for cancer immunotherapy.¹ Along with

WHAT IS ALREADY KNOWN ON THIS TOPIC

⇒ E26 transformation-specific transcription factor ELK3 (ELK3) functions as a master regulator of epithelial-mesenchymal transition to promote cancer metastasis.

WHAT THIS STUDY ADDS

⇒ ELK3 regulates mitochondrial dynamics, which are linked directly to natural killer cell mediated immune responses against triple negative breast cancers.

HOW THIS STUDY MIGHT AFFECT RESEARCH, PRACTICE OR POLICY

⇒ Targeting ELK3 in triple negative breast cancers may increase the immunotherapeutic efficacy of natural killer cells.

T cells, natural killer (NK) cells are major immune effectors that eliminate cancer cells. Due to their potent cytotoxic activity, ability to target cells in an antigen-unrestricted manner, suitability for generation of an allogenic ‘off the shelf’ product, and low risk of toxic side effects (eg, cytokine storm), NK cells are an alternative that might circumvent some of the limitations of CAR T cells.^{2–4}

In patients with cancer, reduced NK cell activity and low infiltration of NK cells into tumor tissues are associated with a worse outcome.^{5–6} Although infusion of activated allogenic or autologous NK cells into patients with myeloid malignancies shows some encouraging clinical results,⁷ the infused NK cells show limited therapeutic efficacy, especially against solid tumors.^{2–3–8–9} Thus, both immune-oncologists and clinicians are seeking to induce immunosensitization of solid tumors to maximize the therapeutic efficacy of NK cells.

Mitochondria are multifunctional organelles whose activity is associated with various

cellular processes, including ATP production via oxidative phosphorylation, calcium homeostasis, reduction-oxidation balance, and induction of programmed cell death.¹⁰ Mitochondria exist in a dynamic state; homeostasis is maintained by striking a balance between fusion and fission in response to the intracellular and extracellular microenvironments.¹¹ Production of reactive oxygen species (ROS) is one of the major physiological processes implicated in mitochondrial dynamics.¹² Mitochondrial fission increases ROS production, and a genetic shift in the mitochondrial balance toward fusion reduces intracellular ROS levels.^{13,14} Eventually, accumulated ROS create a positive feedback loop that regulates mitochondrial dynamics via mitochondrial fusion–fission proteins.^{15,16} Mitochondrial dynamics depend on the activity of dynamin-related GTPase Drp1 (*DNM1L*), and mitochondrial adaptors such as mitochondrial dynamics proteins of 49 and 51 kDa (Mid49 and Mid51).^{17–19} Recent studies demonstrated that Mid51 plays pivotal roles in cancer initiation, progression, metastatic chemotherapy resistance, and poor prognosis.^{20–22} Although Yap–JNK axis, Yap–Hippo axis, and TAZ are known regulators of Mid51 expression in various cancers, including thyroid carcinoma, colorectal cancer, and lung cancer,^{20–23} the transcription factors that directly bind to the Mid51 promoter to regulate its activity have not yet been identified.

E26 transformation-specific transcription factor ELK3 (ELK3) is a ternary complex factor subfamily E26 transformation specific (ETS) protein characterized by its ability to form a ternary nucleoprotein complex with the serum response factor on the serum response element present in the *c-fos* promoter.²⁴ ELK3 functions as a transcriptional repressor that, when phosphorylated, is transformed into a transcriptional activator, leading to vascular endothelial growth factor (VEGF) production and angiogenesis.²⁵ ELK3 plays a pivotal role in the tumorigenesis of various cancers.^{26–31} In squamous cell carcinomas, for example, ELK3 drives malignancy by regulating the chromatin landscape.²⁹ In triple negative breast cancers (TNBCs), ELK3 functions as a master regulator of metastasis by modulating the expression of cancer-associated genes such as VEGFC, GATA3, and E-cadherin.^{26–28} Recently, several studies demonstrated that ELK3 in immune cells, such as macrophages and NK cells, is also involved in the phagocytic or cytotoxic activity of these cells.^{32,33} Despite numerous investigations into the involvement of ELK3 in biological processes, it is currently unknown whether ELK3 expression in cancer is linked to the therapeutic efficacy of immunological treatments.

Previously, we reported that tumors in BALB/c nude mice induced by injection of MDA-MB231 cells with stable knockdown (KD) of ELK3 with shRNA (ELK3KD-231 cells) were significantly smaller than tumors in mice induced by injection with MDA-MB231 control cells, despite the fact that ELK3KD-231 cells had increased *in vitro* proliferation.²⁷

In this study, based on the hypothesis that murine NK cells in BALB/c nude mice inhibit the tumor development

of ELK3KD-231 cells, we show that the level of ELK3 expression in two representative TNBC lines, MDA-MB231 and Hs578T, affects mitochondrial dynamics, resulting in an altered immunological response of these cancers to NK cells. We demonstrate that ELK3 functions as a transcriptional repressor of Mid51, the expression of which is associated directly with mitochondrial fission–fusion and the mitochondrial superoxide concentration in TNBCs. Using molecular and biochemical approaches, we confirmed that the ELK3–Mid51 axis is a major determinant of TNBC immunological responses to NK cells. The data presented herein show that targeting ELK3 in TNBCs can increase the immunotherapeutic efficacy of NK cells.

METHODS

Animal studies

Mice were housed four to five per cage in a semispecific pathogen-free animal facility with controlled temperature and humidity at CHA University (Seongnam-si, Republic of Korea). Briefly, 6-week-old female NSG (NOD-prkdcscid^{em1} Il-2rg^{em1}) mice were purchased from JA bio (Gyeonggi-do, Republic of Korea). After 1 week of acclimatization, the breast cancer orthotopic model was established by inoculating the mice with breast cancer cell lines engineered to express green fluorescence protein and luciferase. MDA-MB231 control, ELK3KD-231, and ELK3KD-231R (restoration of ELK3 expression in ELK3KD-231) cells (5×10^6) were mixed with matrigel (BD Biosciences; dulbecco's phosphate-buffered saline (DPBS)/Matrigel ratio=1) and implanted into the fourth mammary fat pad of each mouse (231 control, n=9; ELK3KD-231, n=9; and ELK3KD-231R, n=8; total n=26). When the tumor volume reached 50–100 mm³, mice were grouped in a Z-shape arrangement depending on tumor size to compare susceptibility of each cancer cell to NK cells. Then, 1×10^7 NK92MI cells or DPBS were injected intratumorally two times per week for 3 weeks (231 control injected by DPBS, n=4; 231 control injected by NK92MI, n=5; ELK3KD-231 injected by DPBS, n=4; ELK3KD-231 injected by NK92MI, n=5; ELK3KD-231R injected by DPBS, n=4; and ELK3KD-231R injected by NK92MI, n=4; total n=26). Tumor size was measured using a vernier caliper two times per week, and the volume was calculated using the following formula: $V \text{ (mm}^3\text{)} = 0.52 \times (\text{tumor length}) \times (\text{tumor width})^2$. Tumor-bearing mice were sacrificed by CO₂ inhalation in a CO₂ chamber on Day 20 postadministration, and tumors were excised for further analysis.

Cell culture

The human breast cancer cell lines MDA-MB231 and Hs578T, and the NK cell line NK92MI, were purchased from the American Type Culture Collection (Manassas, Virginia, USA). MDA-MB231 cells were cultured in Dulbecco's modified Eagle's medium (Gibco, Grand Island, New York, USA) supplemented with 10% fetal

bovine serum and 1% penicillin–streptomycin (Gibco). Hs578T cells were cultured in Dulbecco's modified Eagle's medium (Gibco) supplemented with 10% fetal bovine serum (Gibco), 1% penicillin–streptomycin (Gibco), and 0.01 mg/mL insulin (Sigma, St. Louis, Missouri, USA). NK92MI cells were cultured in Minimum Essential Medium alpha (Gibco) supplemented with 2 mM L-glutamine (Gibco), 1% penicillin–streptomycin (Gibco), 0.1 mM 2-mercaptoethanol (Gibco), 0.02 mM folic acid (Sigma), 0.2 mM inositol (Sigma), and 12.5% fetal bovine serum. Primary NK cells were purified from donor peripheral blood mononuclear cells and were cultured in Advanced Roswell Park Memorial Institute 1640 Medium with Non-Essential Amino Acids (Gibco) supplemented with 10% fetal bovine serum, 1% penicillin–streptomycin, 4 mM GlutaMAX-I Supplement (Gibco), 10 ng/mL human interleukin-2 (PeproTech), and 5 ng/mL interleukin-15 (5 ng/mL; PeproTech) for 2 weeks (14 days). All cells were incubated at 37°C and 5% CO₂.

KD systems and DNA constructs

Stable KD of ELK3 in MDA-MB231 and Hs578T was established by genetic engineering of these cells using retroviruses expressing shRNA targeting ELK3, as described previously.²⁷ Information about the plasmids and small interfering RNAs (siRNAs) is provided in online supplemental table 1.

ROS scavenger and mitochondrial fission inhibitor

N-acetyl cysteine (NAC), an ROS scavenger, was purchased from Sigma (Cat. A7250) and was used at a concentration of 40 mM to pretreat cancer cells at 37°C in a 5% CO₂ atmosphere for 1 hour prior to analysis. Mdivi-1, a small mitochondrial division inhibitor molecule, was purchased from Sigma (Cat. M0199) and used at a concentration of 40 μM to pretreat cancer cells at 37°C in a 5% CO₂ atmosphere for 24 hours prior to analysis.

NK cell-mediated cytotoxicity assay

To analyze the NK cell-mediated cytotoxicity, the activity of extracellular proteases released by dead cell was measured in a CytoTOX-Glo cytotoxicity assay (Promega, Madison, Wisconsin, USA). Cancer cells were seeded into white bottom 96-well plates (1×10⁵ cells per well) and co-cultured with NK92MI cells for 4 hours at the indicated ratios (effector/target (E/T)=10:1, 5:1, 2.5:1, or 1.25:1), after which protease activity was assayed using a luminometer. Cytotoxicity was calculated using the manufacturer's recommended protocol.

To analyze NK-mediated cytotoxicity by flow cytometry, NK cells were first stained with CellTrace CFSE or far-red (Invitrogen, Carlsbad, California, USA) and then co-cultured with target cancer cells for 4 hours at an E/T ratio of 10:1 or 5:1. Next, total cells were stained using 7-aminoactinomycin D (Thermo Fisher Scientific, Rochester, New York, USA), and cell lysis was determined using

a CytoFLEX flow cytometer (Beckman Coulter, Indianapolis, Indiana, USA).

CD107a degranulation assay

To assess degranulation of NK cells, CellTrace CFSE (Invitrogen)-labeled NK92MI cells were co-cultured with target cells for the indicated times at an E:T ratio of 1:1. After harvesting, co-cultured cells were stained with APC mouse antihuman CD107a (BD Biosciences, San Jose, California, USA) for 1 hour at room temperature (RT) and then analyzed using a CytoFLEX flow cytometer (Beckman Coulter).

Apoptosis analysis

For Annexin V/PI staining, NK92MI cells stained with CellTrace CFSE (Invitrogen) were co-cultured with target cancer cells for 4 hours at an E/T ratio of 10:1. Co-cultured cells were stained with APC-Annexin V and PE-PI (BioLegend, San Diego, California, USA) for 15 min. Apoptosis was measured using a CytoFLEX flow cytometer (Beckman Coulter). To detect caspase activity, cancer cells were plated in six-well plates (5×10⁵ cells per well) and then coincubated with NK92MI cells for 4 hours at an E/T ratio of 1:1. Co-cultured cells were washed twice with DPBS to remove NK92MI cells. Then, cancer cells attached to the dish were harvested, and total protein was extracted from the cancer cells for further immunoblot analysis.

Imaging of live cell caspase-3/7 activity

MDA-MB231 and ELK3KD-231 cells were seeded into 96-well plates (2×10⁴ cells per well) and co-cultured for 4 hours with NK92MI cells labeled with CellTrace far-red reagent (Invitrogen). Then, 5 μM CellEvent caspase-3/7 green detection reagent (Invitrogen) was added to the culture medium. After 2 hours, fluorescence images of caspase activity were obtained using the ImageXpress Imaging System (Molecular Devices, San Jose, California, USA).

Detection of ROS and measurement of mitochondrial membrane potential (ΔΨ_m)

To detect intracellular ROS, cells were incubated with 20 μM DCF-DA solution (Abcam, Cambridge, UK) for 30 min at 37°C and then washed with DPBS. Mitochondrial superoxide activity was detected using fluorescent MitoSOX (Invitrogen). Cells were incubated in complete medium containing 5 μM MitoSOX for 30 min at 37°C and then washed with DPBS. To measure the ΔΨ_m, cells were incubated for 30 min at 37°C with 10 μg/mL of JC-1 (Invitrogen) and then washed with DPBS. Fluorescence was assessed in a CytoFLEX flow cytometer (Beckman Coulter).

RNA extraction and quantitative RT-PCR

Total RNA was extracted from cells using TRIzol (Invitrogen), and complementary DNA (cDNA) was synthesized from 1 μg of total RNA using the LeGene 1st Strand cDNA Synthesis System (LeGene Biosciences, San Diego,

California, USA). Quantitative PCR was performed using TOPreal qPCR 2X PreMIX (Enzynomics, Daejeon, Chungnam, Republic of Korea) and the CFX Connect Real-Time PCR Detection System (Bio-Rad, Hercules, California, USA). The primers used in this study are listed in online supplemental table 2.

Immunoblot analysis

Cells were mixed with cell lysis buffer (Cell Signaling) containing a protease and phosphatase inhibitor cocktail (Thermo Fisher Scientific) and then heated for 10 min at 95°C. Cell lysates were resolved in sodium dodecyl sulfate-polyacrylamide gels, and the separated proteins were transferred to polyvinylidene difluoride membranes (Bio-Rad). Membranes were blotted with the indicated antibodies, and immunoreactivity was detected using the enhanced chemiluminescence solution (Thermo Fisher Scientific). The antibodies used in this study are listed in supplementary online supplemental table 3.

Chromatin immunoprecipitation and quantitative chromatin immunoprecipitation assays

Cells were fixed in 1% paraformaldehyde solution and incubated for 15 min at RT to cross-link proteins and genomic DNA. Glycine was added to a final concentration of 125 mM to quench the formaldehyde. After incubating for 15 min at room temperature, cells were washed with phosphate buffered saline and lysed with cell lysis buffer (Cell Signaling) containing protease/phosphatase inhibitors (Thermo Fisher Scientific). Cell lysates were sonicated to fragment genomic DNA and then centrifuged at 15,000×g for 15 min at 4°C. The supernatants were mixed with protein A/G magnetic beads (Thermo Fisher Scientific) and incubated with primary antibodies overnight at 4°C. The complexes were washed sequentially with 1×radioimmunoprecipitation assay (RIPA) buffer, 1×RIPA buffer (300 mM NaCl), LiCl buffer, and TE buffer. To separate the DNA-protein complexes, SDS and proteinase K were added. Immunoprecipitated DNA was purified using the phenol/chloroform extraction method, prior to use in chromatin immunoprecipitation (ChIP)-quantitative PCR. The amount of precipitated chromatin was calculated as a percentage of the input sample. All experiments were performed in triplicate.

Measurement of mitochondrial length

Cells were seeded in a 96-well black/clear bottom plate (1×10^4 per well). Cells were incubated for 30 min at 37°C with 1 μM of MitoTracker Green (Invitrogen) and then washed with DPBS. Cells stained with MitoTracker were imaged under a fluorescence microscope (EVOS M5000 imaging system; Thermo Fisher Scientific). The length of the mitochondria was measured by ImageJ.

Transmission electron microscopy

Cancer cells were fixed with 2.5% glutaraldehyde at 4°C for 8 hours and then fixed in 1% osmium tetroxide for 1 hour. After washing, samples were dehydrated by sequential washes in 60%, 70%, 90%, 95%, and 100%

ethanol solutions, and embedded in epon resin. Then, samples were cut into thin sections, and counterstained with uranyl acetate and lead citrate. Images were acquired under a transmission electron microscope (H-7600; Hitachi, Tokyo, Japan).

RNA-sequencing and ChIP-sequencing analysis

For gene expression profiling, sequencing libraries were prepared using the QuantSeq 3' mRNA-Seq kit (Ebiogen, Seoul, Republic of Korea). Gene expression patterns were analyzed using ExDEGA software (Excel Based Differentially Expressed Gene Analysis, Ebiogen).

Library preparation for ChIP-sequencing (ChIP-seq) was performed using the NEBNextUltra™ DNA Library Prep Kit for Illumina (New England Biolabs, UK). Briefly, the methylated DNA fragment was ligated using adaptors. After purification, the ligated DNA-adaptor and index primer for multiplexing sequencing were used for the PCR reaction. To remove all reaction components, the library was purified on magnetic beads. The size of library was assessed by an Agilent 2100 Bioanalyzer (Agilent Technologies, Amstelveen, the Netherlands). High-throughput sequencing was conducted by single-end 75 sequencing using NextSeq 500 (Illumina, USA). Prior to aligning to the genome and transcriptome, the reads were trimmed and aligned using Bowtie2. Bowtie2 indices were generated from either genome assembly sequences or representative transcript sequences. MACS (Model-based Analysis of ChIP-Seq) was used to identify peaks from the alignment file. Gene classification was based on searches of the MEDLINE database. The RNA sequencing (RNA-seq) and ChIP-seq data reported in this article have been deposited in National Center for Biotechnology Information (NCBI)'s Gene Expression Omnibus (GEO) (RNA-seq; GSE197575 and ChIP-seq; GSE197572).

Luciferase assay

The *Mid51* promoter sequence (−100 to 0) with either the wild type or mutant *ELK3* binding motif was synthesized by Bioneer (Daejeon, Chungnam, Republic of Korea) and cloned downstream of the SV40 promoter in the pGL3-control plasmid. *ELK3KD* MDA-MB231 cells were transfected with the indicated plasmids using Lipofectamine 2000 (Invitrogen). Transfected cells were harvested 48 hours after transfection and lysed using cell lysis buffer (Cell Signaling). Luciferase activity was measured using the Dual-Luciferase Reporter Assay System (Promega). The values for firefly luciferase activity were normalized to the respective values of Renilla luciferase activity.

Bioinformatics analysis of public breast cancer data sets

To assess the correlation between *ELK3* and *Mid51* expression in breast cancer cell lines, microarray data were downloaded from the GEO database under access codes GSE41313.³⁴ For bioinformatics analysis of *ELK3* and *Mid51* expression in patients with TNBC, METABRIC breast cancer data were downloaded from cBioPortal on September 1, 2021.³⁵ Patients were filtered by selecting

cases with ‘negative’ estrogen receptor status, ‘negative’ progesterone receptor status, a ‘claudin-low, basal’ PAM50-subtype, and a cancer type described as ‘Breast invasive ductal carcinoma’. By merging clinical data with gene expression data, 236 TNBC cases were selected. Kaplan-Meier analysis was performed to compare overall survival and relapse-free survival according to the negative correlated expression levels of *ELK3* and *Mid51*. Patients with TNBC with *ELK3* expression in the top 15% and *Mid51* expression in the bottom 15% were labeled as ‘*ELK3*^{High} and *Mid51*^{Low},’ while patients with TNBC with *ELK3* expression in the bottom 15% and *Mid51* expression in the top 15% were labeled as ‘*ELK3*^{Low} and *Mid51*^{High}’. All survival analyses were performed in R V.4.1.1 (<https://www.R-project.org>) using the *survminer* and *survival* R packages.³⁶ For NK score analysis, the *deconvolute* function of *immunedevconv* R package was used with the following parameters: *method* = ‘*quantiseq*’; *arrays*=T0.³⁷

Statistical analysis

Statistical analyses were performed using GraphPad Prism V.7.0 software (GraphPad Software, La Jolla, California, USA). The statistical significance of differences was determined by an unpaired Student’s t-test. The results of the in vivo tumor growth study were analyzed using two-way analysis of variance. Graphical data are presented as the mean±SD from at least three independent experiments, each with triplicate samples. Pearson’s correlation analysis was used to evaluate the correlation between expression of *ELK3* and *Mid51*. Survival curves were generated using the Kaplan-Meier method, and differences were assessed using the log-rank test. P values<0.05 were considered statistically significant.

RESULTS

Suppressing ELK3 restores susceptibility of TNBC cells to NK cells

Previously, we reported that tumors in BALB/c nude mice after stable KD of ELK3 with shRNA in MDA-MB231 cells (ELK3KD-231 cells) are significantly smaller than control MDA-MB231 tumors, despite the fact that ELK3KD-231 cells showed increased proliferation in vitro.²⁷ Since murine NK cells are active in BALB/c nude mice,^{38,39} we questioned whether NK cell depletion in BALB/c nude mice might affect the tumor development of MDA-MB231. As shown in online supplemental figure S1, ELK3KD-231 formed larger tumors in BALB/c nude mice when NK cells were depleted by continuous injection of anti-asialo-GM1 antibody into the mice. Based on these findings, we hypothesized that development of ELK3KD-231 tumors was inhibited by murine NK cells. Thus, we investigated whether the level of ELK3 expression in two representative human TNBC lines, MDA-MB231 and Hs578T, influences in vitro antitumor NK cell responses. As shown in figure 1A, the number of lysed cells of ELK3KD Hs578T (ELK3KD-578T) and ELK3KD-231

cells was significantly higher than that in control cells at all E:T ratios tested. In co-cultures of ELK3KD-231 and ELK3KD-578T cells, the frequency of degranulated CD107a⁺ NK92MI cells was greater than that of control cells (figure 1B). Primary NK cells, like NK92MI cells, caused ELK3KD-231 and ELK3KD-578T cells to lyse up to 1.5-fold more than control cells (figure 1C).

When ELK3KD-231 or control MDA-MB231 cells were engrafted into NSG mice, which lack NK cells, T cells, and B cells, the resulting ELK3KD-231 tumors were markedly larger than control tumors; also, intratumoral injection of NK92MI significantly impaired the development of ELK3KD-231 tumors (data not shown).

Since the mechanism underlying NK cell-mediated killing of target cells comprises a mixture of necrosis and caspase-dependent apoptosis,⁴⁰ we next asked which type of cell death is associated with the enhanced response of ELK3KD TNBCs to NK cells. Annexin V/PI staining revealed that the rapid lysis of ELK3KD-231 cells mediated by NK92MI cells was mainly attributable to induction of late apoptosis (Annexin V⁺/PI⁺) (figure 1D). Immunoblot analysis of cleaved caspase-3 and -9 supported the rapid activation of apoptosis in ELK3KD-231 exposed to NK92MI cells (figure 1E). Time-lapse monitoring of a fluorescent indicator of caspase-3/7 activity further revealed rapid activation of caspase-3/7 in ELK3KD-231 cells following coincubation with NK92MI cells (figure 1F). Consistent with this, genome-wide expression profiling and qRT-PCR analysis showed that expression of pro-survival and proapoptosis genes was disrupted markedly in ELK3KD-231 and ELK3KD-578T cells (online supplemental figure S2). Considering that the susceptibility of cancer cells to apoptotic stimuli is affected by the balance between pro- and antiapoptotic proteins,⁴¹ these results suggest that knocking down ELK3 reprograms TNBCs to become more sensitive to external apoptotic stress.

Mitochondrial fission-mediated superoxide accumulation increases susceptibility of ELK3-suppressed TNBCs to NK cells

Previously, we reported that ELK3KD-231 cells proliferated faster than control cells in vitro.²⁷ Because tumor cell proliferation is linked to intracellular ROS production,⁴² we next examined cytoplasmic ROS levels in ELK3KD TNBCs. As expected, intracellular ROS accumulation was significantly higher in ELK3KD-231 and ELK3KD-578T cells than in control cells (figure 2A).

Based on a report that cytotoxic lymphocytes induce target cell death by triggering ROS-dependent apoptosis,⁴³ we hypothesized that elevated cytoplasmic ROS levels would increase the vulnerability of ELK3KD TNBCs to NK cells. Indeed, the sensitivity of ELK3KD-231 and ELK3KD-578T to NK92MI cells was reduced, similar to that of control cells, in the presence of NAC, which scavenges intracellular ROS (online supplemental figure S3A, figure 2B). Consistently, the degree of NK92MI-mediated cleavage of caspase-3 and caspase-9 in ELK3KD-231 and ELK3KD-578T cells treated with NAC was lower

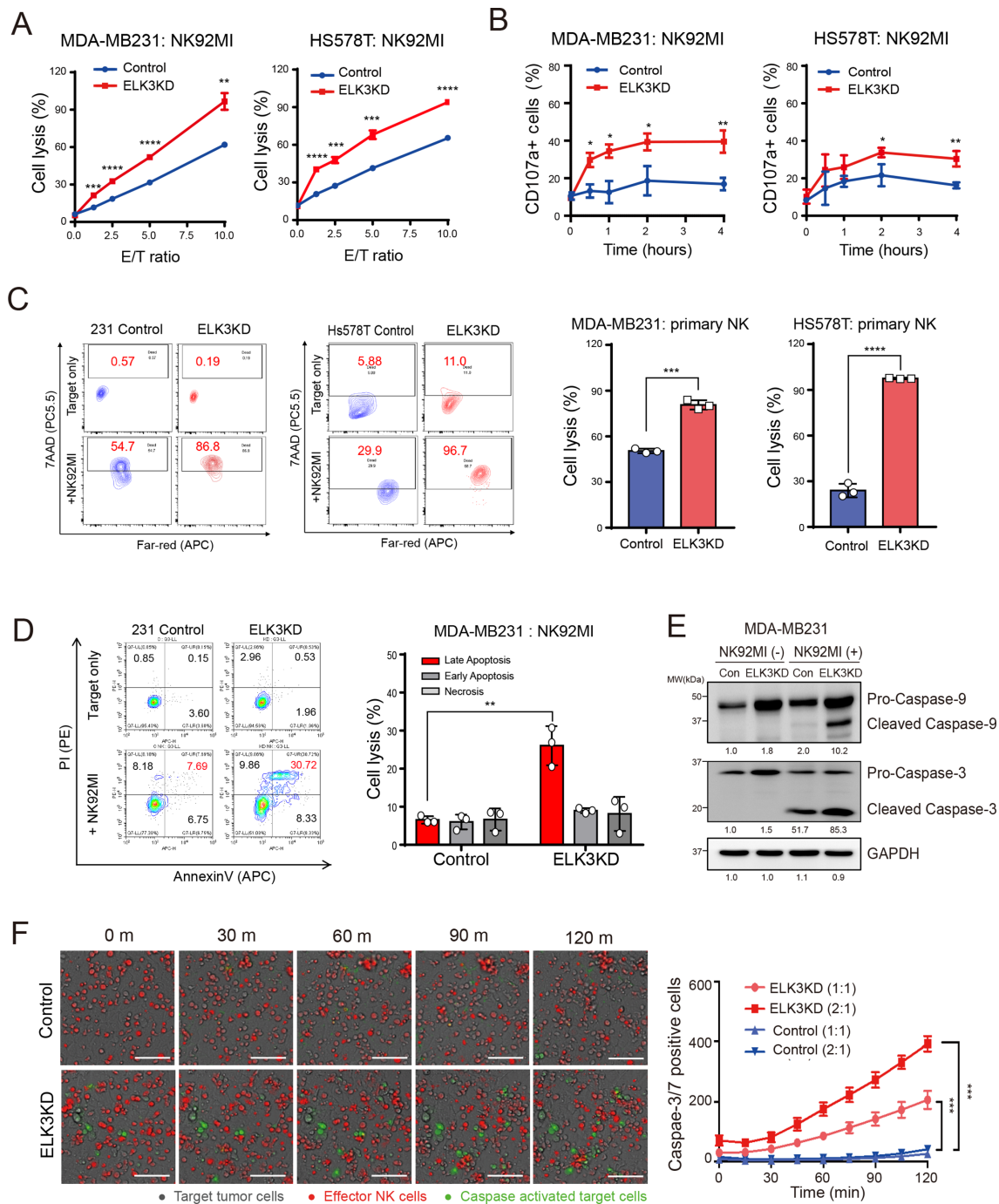


Figure 1 Suppression of ELK3 reprograms triple negative breast cancer cells to be susceptible to NK cells. (A) A CytoTOX-Glo assay was performed to quantify lysis of ELK3KD-231 and ELK3KD-578T cells incubated with NK92MI for 4 hours at the indicated E/T ratios (NK92MI cells/target cells). (B) Degranulation of NK92MI cells co-cultured with ELK3KD-231 and ELK3KD-578T cells for the indicated times. The E/T ratio in this experiment was 1. (C) Far-red-7AAD assay to quantify lysis of ELK3KD-231 and ELK3KD-578T cells incubated with primary NK cells for 4 hours at an E/T ratio of 5 (NK92MI cells/target cells). (D) Comparison of early and late apoptosis of MDA-MB231 and ELK3KD-231 cells incubated with NK92MI for 4 hours at an E/T ratio of 10:1. Apoptosis was evaluated by Annexin V/PI staining (Annexin V⁺/PI⁺, necrosis; Annexin V⁺/PI⁻, early apoptosis; Annexin V⁻/PI⁺, late apoptosis). (E) Immunoblot analysis of cleaved caspase-3 and caspase-9 expression in MDA-MB231 and ELK3KD-231 cells incubated with NK92MI for 4 hours at an E/T ratio of 1:1. GAPDH was used as a loading control. The band intensities on the immunoblot were measured using ImageJ, and the results are displayed beneath the blot. (F) (left) Real-time detection of caspase-3/7 activity in MDA-MB231 and ELK3KD-231 cells incubated with NK92MI for the indicated times at an E/T ratio of 2:1. (right) The number of green cancer cells expressing active caspase-3/7 activity was counted at the indicated times. Control=wildtype MDA-MB231 or Hs578T cells; ELK3KD=ELK3KD-231 or ELK3KD-578T cells. Scale bar, 200 μ m. All of experiments were performed in triplicate. P values were calculated by a two-tailed Student's t-test ((A)–(D) and (F)). Data represent the mean \pm SD. *, $p < 0.05$; **, $p < 0.01$; ***, $p < 0.001$; ****, $p < 0.0001$. ELK3, transcription factor; E:T, effector:target; NK, natural killer; ns, non-significant; 7-AAD, 7-aminoactinomycin D.

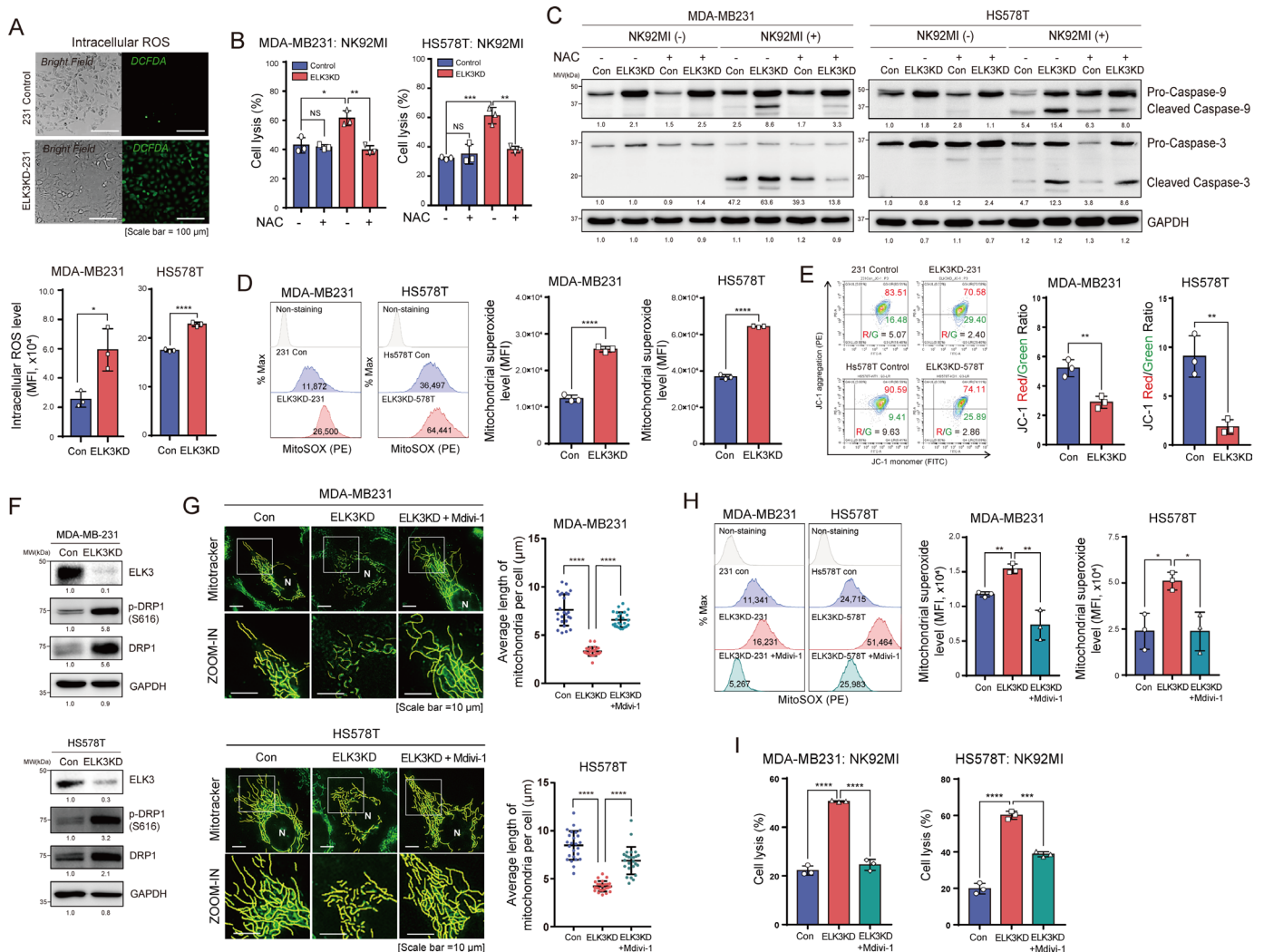


Figure 2 Mitochondrial fission-mediated superoxide accumulation increases susceptibility of ELK3-suppressed TNBCs to NK cells. (A) (upper) Representative images of DCF-DA staining of intracellular reactive oxygen species (ROS) levels in the MDA-MB231 control and ELK3KD-231 cells. Scale bar, 100 μ m. (lower) Quantification of the results of DCF-DA staining of intracellular ROS of the indicated cells through flow cytometry. (B) CFSE-7AAD assay to quantify lysis of ELK3KD-231 and ELK3KD-578T cells incubated with NK92MI for 4 hours at an E:T ratio 10:1 in the presence or absence of the ROS scavenger N-acetyl-L-cysteine (NAC). (C) Immunoblot analysis of cleaved caspase-3 and caspase-9 levels in target cells incubated with NK92MI in the presence or absence of NAC for 4 hours at an E/T ratio of 1:1. Quantification of cleaved caspase-3 and caspase-9 was performed using ImageJ. The data are shown under the blot. (D) (left) Histogram and (right) quantification of the results of MitoSOX staining of mitochondrial superoxide of the indicated cells through flow cytometry. (E) JC-1 staining of mitochondrial membrane potential in control and ELK3KD cells. (F) Immunoblot analysis of phosphorylated DRP1 (S616) and total DRP1 expression in ELK3KD-231 and ELK3KD-578T cells. Quantification of protein expression was performed by ImageJ, and the data are presented under the blot. (G) Imaging of mitochondrial morphology by MitoTracker staining of indicated control, ELK3KD, and ELK3KD cells treated with a mitochondrial fission inhibitor, Mdivi-1. Average length of mitochondria per cell was measured in 25 cells per group. The data are presented as a graph. Scale bar, 10 μ m. (H) Measurement of mitochondrial superoxide levels in control, ELK3KD, and ELK3KD cells treated with Mdivi-1. (I) CFSE-7AAD assay to quantify lysis of control, ELK3KD, and ELK3KD cells treated with Mdivi-1 and incubated with NK92MI for 4 hours at an E:T ratio of 10:1. Control=wild type MDA-MB231 or Hs578T cells; ELK3KD=ELK3KD-231 or ELK3KD-578T cells. P values were calculated by a two-tailed Student's t-test ((A), (B), (D), (E) and (G)–(I)). Data represent the mean \pm SD. All experiments were performed in triplicate. *, $p < 0.05$; **, $p < 0.01$; ***, $p < 0.001$; ****, $p < 0.0001$. ELK3, transcription factor; E:T, effector:target; NK, natural killer; ns, non-significant; TNBC, triple negative breast cancer; 7-AAD, 7-aminoactinomycin D; CFSE, carboxyfluorescein succinimidyl ester; DCF-DA; 2',7'-dichlorodihydrofluorescein diacetate.

than that of the NAC-untreated group (figure 2C). These results indicate that high levels of intracellular ROS in ELK3KD TNBCs sensitize cells to the cytotoxic effects of NK cells. Next, we confirmed that accumulated

ROS in ELK3-suppressed TNBCs is derived mainly from mitochondria, rather than lipids (figure 2D, online supplemental figure S3B, C). The decreased mitochondrial membrane potential ($\Delta\Psi$ m) in ELK3KD-231 and

ELK3KD-578T cells indicates that excessive ROS are associated with mitochondrial status (figure 2E, online supplemental figure S3D). To understand the mechanism underlying the low $\Delta\Psi_m$ and high mitochondrial superoxide levels in ELK3KD-231 and ELK3KD-578T cells, we noted that mitochondrial morphology and function are linked, and that mitochondrial fragmentation affects $\Delta\Psi_m$ as well as mitochondrial ROS generation.^{15,44} Since mitochondria are in a constant state of fusion and fission, and exist either as a fused tubular network or in a fragmented state depending on the cellular state,⁴⁵ we next examined whether ELK3 suppression affected mitochondrial dynamics in MDA-MB231 and Hs578T cells.

As shown in figure 2F, the amount of total and phosphorylated DRP1 (S616), which mediates mitochondrial fission, increased in ELK3-suppressed TNBCs. Consistent with this, we found that mitochondria in ELK3KD-231 and ELK3KD-578T cells were significantly shorter than those in control cells, and that treatment with mdivi-1 (mitochondrial fission inhibitor 1) restored the length of the mitochondria to control levels (figure 2G). In the presence of mdivi-1, the increased mitochondrial superoxide levels in ELK3KD TNBCs were also attenuated to control levels (figure 2H, online supplemental figure S3E). Consistent with this, treatment with mdivi-1 reduced the susceptibility of ELK3KD-231 and ELK3KD-578T cells to NK cell-mediated cytotoxicity (figure 2I). Taken together, the data suggest that the imbalance between fusion and fission dynamics (ie, elevated fission activity) generates mitochondrial superoxide, and makes ELK3KD-231 and ELK3KD-578T more susceptible to NK cells.

Restoration of ELK3 expression reverses the immunosensitivity of ELK3-suppressed TNBCs

To demonstrate that ELK3 actively regulates mitochondrial dynamics and the responses of TNBCs to NK cells, we transiently rescued ELK3 expression in ELK3KD-231 and ELK3KD-578T cells (figure 3A) and then examined the effects on NK responses. As shown in figure 3B, ELK3 restoration in ELK3KD-231 and ELK3KD-578T cells resulted in greater resistance to NK92MI. In line with this, elevated levels of mitochondrial superoxide in ELK3KD-231 and ELK3KD-578T cells fell back to control levels (figure 3C). Electron microscopy observations of mitochondria in MDA-MB231 cells further confirmed that mitochondrial length, which was short in ELK3KD-231 cells, was significantly elongated by restoration of ELK3 expression (figure 3D). These data suggest that ELK3 expression level is associated with mitochondrial dynamics.

To verify that ELK3 also determines the immunosensitivity of TNBCs to NK cells in vivo, we engineered ELK3KD-231 cells to be rescued by ELK3 expression in a stable manner (ELK3KD-231R) (online supplemental figure S4A, B). Then, we established an orthotopic mammary fat pad mouse model by grafting control, ELK3KD-231, and ELK3KD-231R cells into NSG mice, followed by injection of NK92MI cells directly into the tumors

(figure 3E). The body weights of the control, ELK3KD-231, and ELK3KD-231R mice did not change appreciably after administration of DPBS or NK92MI (online supplemental figure S4C). Despite the fact that ELK3KD-231 cells generated larger tumors than those of the control or ELK3KD-231R cells, the growth of ELK3KD-231 cell tumors was greatly decreased by the injection of NK92MI, in contrast to tumors of control or ELK3KD-231R cells, whose growth was not altered by the injection of NK92MI (figure 3F–3H).

Immunohistochemical staining of cleaved caspase-3 in tumors excised from each group supported the notion that apoptosis of tumor cells was severe only in ELK3KD-231 tumors after NK92MI treatment (figure 3I). Consistent with the in vitro result (figure 3C), figure 3J shows that the amount of mitochondrial superoxide accumulated in ELK3KD-231 tumors was significantly higher than that in ELK3KD-231R tumors. These data indicate that ELK3 expression levels determine mitochondrial dynamics in TNBCs, which are linked directly to mitochondrial superoxide generation and immune sensitivity to NK cells, both in vitro and in vivo.

ELK3 functions as a transcriptional repressor of Mid51 in TNBCs, and the ELK3-Mid51 axis determines tumor cell responses to NK cells

Next, we employed genome-wide ChIP-seq and RNA-seq analysis of MDA-MB231, ELK3KD-231, and ELK3KD-231R cells to screen downstream targets of ELK3. Among 5002 potential targets of ELK3 identified by ChIP-seq analysis, 287 were sorted as mitochondria-related genes by the MitoCarta database (online supplemental figure S5A). Combined gene ontology analysis of the RNA-seq results for the 287 genes identified 6 genes (*BNIP3*, *PINK1*, *DNM1L*, *Mid51*, *MUL1*, and *FIS1*) encoding positive regulators of mitochondrial fission (online supplemental figure S5B). Considering that suppression of ELK3 results in mitochondrial fission, we would expect that ELK3 functions as a transcriptional repressor of positive regulators of mitochondrial fission in TNBC, and that target gene expression correlates negatively with ELK3. Four genes (*DNM1L*, *Mid51*, *MUL1*, and *FIS1*) from the RNA-seq analysis fit these criteria, and all have an ELK3 binding motif in the promoter region near the transcription initiation site (+1) (online supplemental figure S5B, C). Quantitative RT-PCR and immunoblot analysis showed that enhanced expression of *Mid51* and *DNM1L* in ELK3KD-231 and ELK3KD-578T was suppressed by restoration of ELK3 expression (figure 4A and B). Nevertheless, although the ELK3 binding motif near the transcription initiation site (+1) is conserved in the *Mid51* promoter of human, murine, rat, and zebrafish, it is not conserved in the *DNM1L* promoter (figure 4C). Therefore, we focused on *Mid51*. *Mid51* encodes a mitochondrial dynamics protein of 51 kDa that functions as an adaptor protein for dynamin-related protein 1 (Drp1).¹⁹ Recruitment of Drp1 by *Mid51* to the mitochondrial outer membrane results in mitochondrial fission.⁴⁶

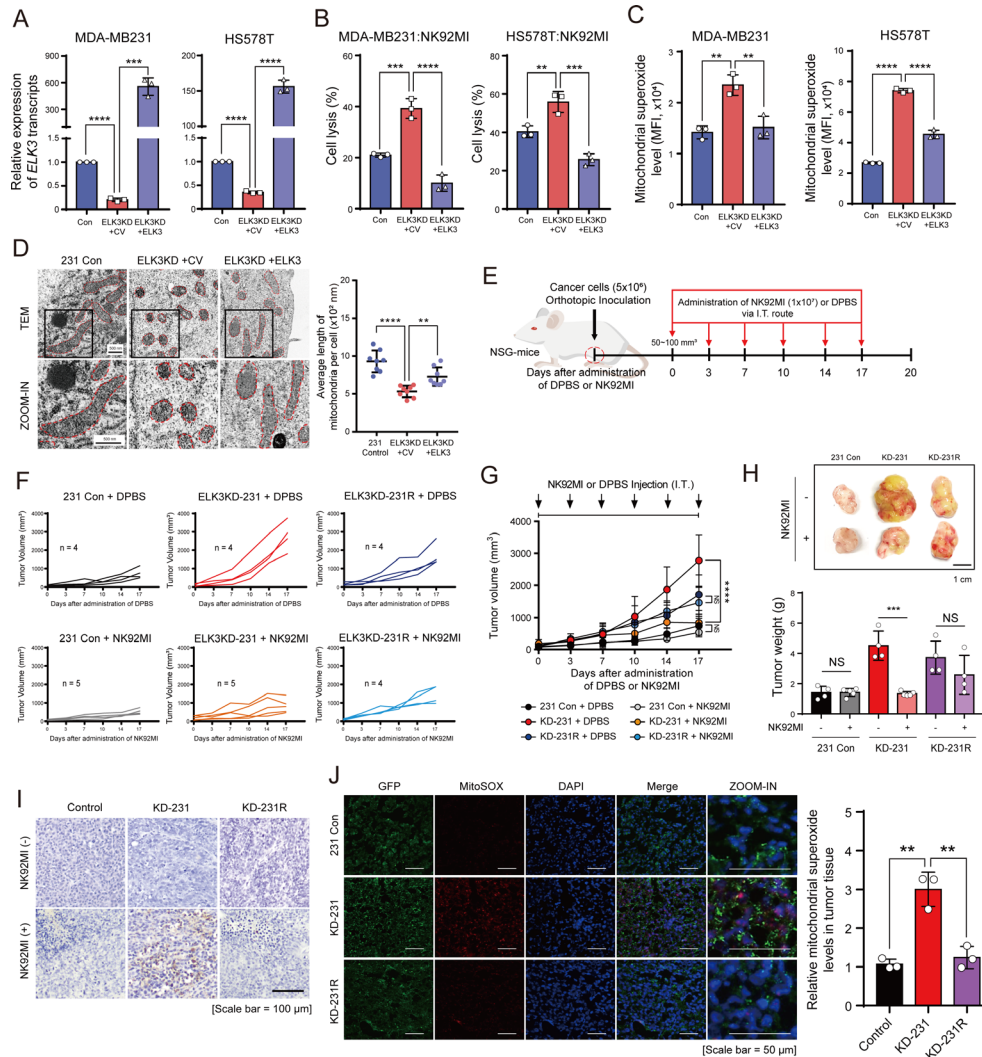


Figure 3 Restoration of ELK3 reverses the sensitivity of ELK3-suppressed TNBCs to NK cells in vitro and in vivo. (A) Quantitative RT-PCR analysis of ELK3 expression in control and ELK3KD TNBCs transfected for 48 hours with a control plasmid or an ELK3-expressing plasmid. (B) Far-red-7AAD assay to quantify lysis of control and ELK3KD TNBCs transfected for 48 hours with a control plasmid or an ELK3-expressing plasmid. NK92MI and target cells were co-cultured for 4 hours at an E:T ratio of 10:1. (C) Measurement of mitochondrial superoxide in control and ELK3KD TNBCs transfected for 48 hours with a control plasmid or an ELK3-expressing plasmid. (D) (left) Representative electron microscopic image of mitochondria in control MDA-MB231, ELK3KD-231, and ELK3KD-231 cells transfected for 48 hours with an ELK3-expressing plasmid. The average length of mitochondria per cell was measured in eight cells per group. (right) The data are presented as a graph. Scale bar, 500 nm. (E) Experimental scheme. MDA-MB231, ELK3KD-231, and ELK3KD-231R cells, which were engineered to express GFP and luciferase, were injected orthotopically into the mammary fat pad of NSG mice (5×10^6 cells per mouse). After tumor size reached 50–100 mm^3 , NK92MI cells (1×10^7) or DPBS was injected intratumorally two times per week for 3 weeks (MDA-MB231 control injected by DPBS, $n=4$; MDA-MB231 control injected by NK92MI, $n=5$; ELK3KD-231 injected by DPBS, $n=4$; ELK3KD-231 injected by NK92MI, $n=5$; ELK3KD-231R injected by DPBS, $n=4$; and ELK3KD-231R injected by NK92MI, $n=4$; total $n=26$). (F) Tumor growth curves from individual mice in each group bearing MDA-MB231 (Control), ELK3KD-231, or ELK3KD-231R tumors treated with DPBS or NK92MI for the indicated times. (G) Average tumor growth curves for mice bearing MDA-MB231 (Control), ELK3KD-231, or ELK3KD-231R tumors treated with DPBS or NK92MI for the indicated times. The significance of differences between the DPBS and NK92MI-treated groups was calculated. (H) (upper) Representative tumors from each group, and (lower) quantitation of average tumor weight at 20 days after administration of DPBS or NK92MI. Scale bar, 1 cm. (I) Representative images of the results of immunohistochemical analysis of cleaved caspase-3 in sections of xenograft tumors of three mice per group. Scale bar, 100 μm . (J) Mitochondrial superoxide levels in sections of tumor xenografts. (left) Sections were stained and subjected to immunofluorescence analysis with MitoSOX (right), and immunofluorescence was measured in sections of tumors of three mice per group using ImageJ. Cancer cells were labeled as a GFP. Scale bar, 50 μm . All experiments were conducted in triplicate, and data represent the mean \pm SD. P values were calculated by a two-tailed Student's t-test ((A)–(D), (H), and (J)) or two-way analysis of variance (G). For the in vivo experiments, four or five mice per group were used. * $p < 0.05$; ** $p < 0.01$; *** $p < 0.001$; **** $p < 0.0001$. ELK3, transcription factor; E:T, effector:target; GFP, green fluorescence protein; NK, natural killer; ns, non-significant; TNBC, triple negative breast cancer; 7-AAD, 7-aminoactinomycin D; DPBS, dulbecco's phosphate-buffered saline; RT, reverse transcription.

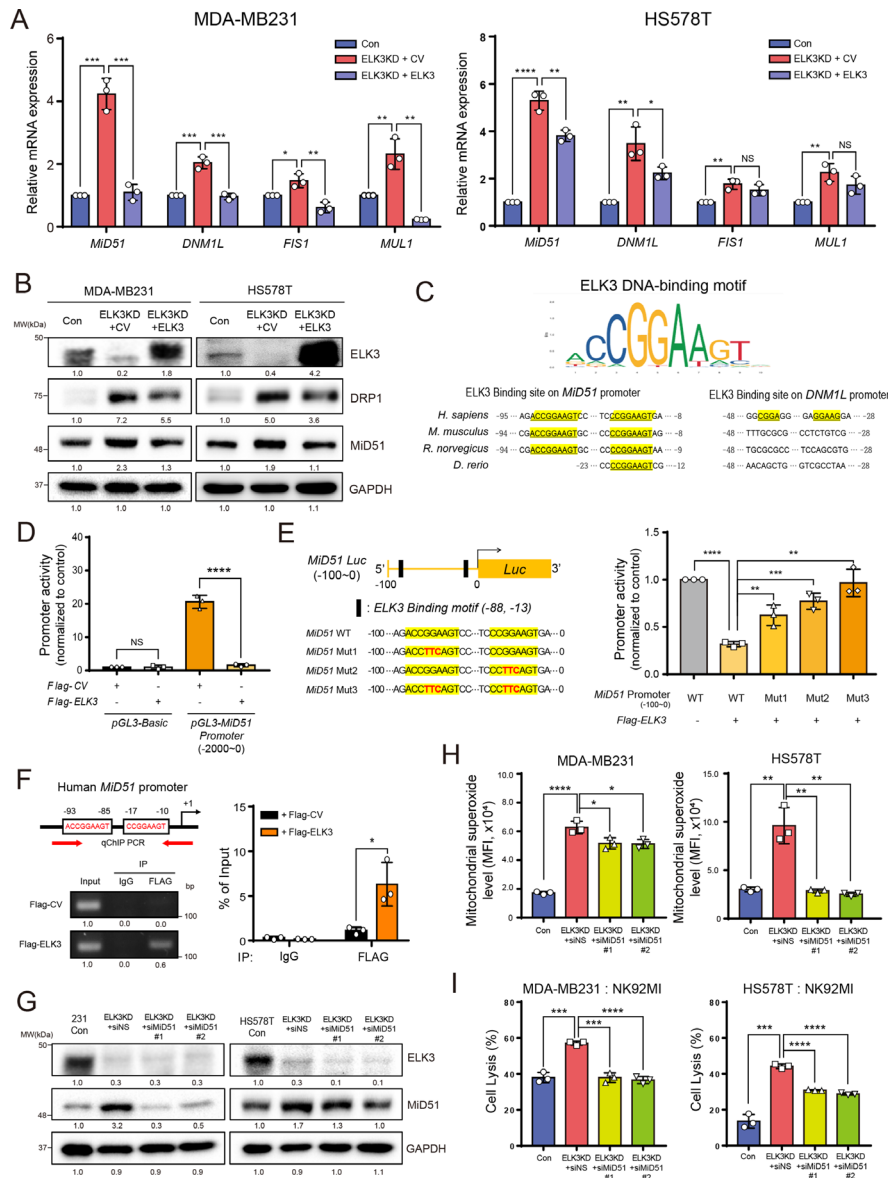


Figure 4 ELK3 is a transcriptional repressor of Mid51, and the ELK3-Mid51 axis determines the response of TNBCs to NK cells. (A) Quantitative RT-PCR analysis of *Mid51*, *DNMT1L*, *FIS1*, and *MUL1* expression in control and ELK3KD TNBCs transfected with a control plasmid or an ELK3-expressing plasmid. (B) Immunoblot analysis of Drp1 and Mid51 expression by control and ELK3KD TNBCs transfected with a control plasmid or an ELK3-expressing plasmid. (C) Phylogenetic sequence comparison of the Mid51 and DNMT1L proximal promoter regions from human, mouse, rat, and zebrafish. The conserved ELK3 binding site is highlighted in yellow. (D) Luciferase assay of the pGL3 reporter plasmid harboring the Mid51 promoter region (–2 kb to 0 bp). The reporter plasmid, the control plasmid (Flag-CV), and the ELK3-expressing plasmid (Flag-ELK3) were transfected into ELK3KD-231 cells as indicated. (E) (left) Schematic of the luciferase reporter plasmid harboring the promoter region (–100 to 0 bp) of Mid51 downstream of the SV40 promoter from the pGL3-control plasmid. ELK3 binding sequences (in red) were mutated as described to produce M1, M2, and M3. (right) Luciferase activity of the fused promoter in ELK3KD-231 cells cotransfected with the indicated reporter plasmid in the presence or absence of an ELK3-expressing plasmid. (F) ChIP-qPCR analysis of ELK3 binding to the Mid51 promoter. Flag-ELK3-expressing plasmid was transfected into ELK3KD-231 cells, and Flag-immunoprecipitates were subjected to qPCR using primers specific for the Mid51 promoter region (–116 to 24 bp). (G) Immunoblot analysis of Mid51 in control and ELK3KD TNBCs transfected with a non-specific or Mid51-targeting siRNA. Band intensities on the immunoblot were measured by ImageJ, and the results are displayed beneath the blot. (H) Measurement of mitochondrial superoxide in control and ELK3KD TNBCs transfected with a non-specific or Mid51-targeting siRNA. (I) CFSE-7AAD assay to quantify lysis of control and ELK3KD TNBCs transfected with a non-specific or Mid51-targeting siRNA. NK92MI and target cells were co-cultured for 4 hours at an E:T ratio of 10:1. All assays were performed in triplicate. P values were calculated by a two-tailed Student's t-test ((A), (D)–(F), (H), and (I)). Data represent the mean \pm SD. *, $p < 0.05$; **, $p < 0.01$; ***, $p < 0.001$; ****, $p < 0.0001$. ChIP, chromatin immunoprecipitation; ELK3, transcription factor; E:T, effector:target; Mid51, mitochondrial dynamics proteins of 51; NK, natural killer; ns, non-significant; qPCR, quantitative PCR; TNBC, triple negative breast cancer; 7-AAD, 7-aminoactinomycin D; siRNA, small interfering RNA; RT, reverse transcription; CFSE, Carboxyfluorescein succinimidyl ester.

To verify that *Mid51* is a direct target of *ELK3*, we next employed a luciferase reporter assay using a cloned *Mid51* promoter. As expected, activity of the *Mid51* promoter in *ELK3KD-231* cells was repressed significantly by *ELK3* (figure 4D). Because the *ELK3* binding motif is close to the transcription initiation site of the *Mid51* promoter, we questioned whether *ELK3* represses transcription of *Mid51* via steric hindrance. We tested this possibility using a pGL3 reporter plasmid harboring a 100bp sequence of the *Mid51* promoter (which includes two *ELK3* binding sequences at -88 and -13 downstream of the SV40 promoter (figure 4E, left panel)). As expected, cotransfection of the *ELK3* plasmid led to a significant decrease in luciferase expression from the reporter plasmid harboring wild-type *ELK3* binding sequences, but not from that harboring mutated sequences (figure 4E, right panel). The results of a ChIP assay further demonstrated that ectopically expressed *ELK3* bound directly to the *Mid51* promoter in *ELK3KD-231* cells (figure 4F). Lastly, we analyzed the effect of siRNA-mediated suppression of *Mid51* (siMid51) on mitochondria status and immunosensitivity of *ELK3KD* TNBCs. When siMid51 was transfected into *ELK3KD-231* and *ELK3KD-578T* cells, those cells became less susceptible to NK cells, and mitochondrial superoxide accumulation decreased (figure 4G–I). Electron microscopy of the dynamics of mitochondria showed that the shortness of the mitochondria in *ELK3KD-231* cells was significantly reduced when high expression of *Mid51* in *ELK3KD-231* was suppressed with siMid51 (online supplemental figure S6A). Also, mitochondrial membrane potential was rescued when *ELK3KD-231* and *ELK3KD-578T* cells were transfected with siMid51 (online supplemental figure S6B). These results suggest that *ELK3* is a transcriptional repressor of *Mid51*, and that the *ELK3-Mid51* axis modulates TNBC responses to NK cells by modulating mitochondrial dynamics and ROS accumulation.

The *ELK3-Mid51* axis plays a role in NK cell immunosurveillance and in survival of patients with TNBC

To clarify the association between *ELK3* expression and *Mid51*, we performed a bioinformatics analysis of *ELK3* and *Mid51* expression patterns in breast cancer cell lines and patient samples. As shown in figure 5A, expression of *ELK3* correlated negatively with that of *Mid51* in 23 TNBC cell lines (GSE41313). Likewise, analysis of 263 patients with TNBC from the METABRIC database revealed that expression of *ELK3* showed a weak but statistically significant negative correlation with that of *Mid51* (figure 5B). In order to examine the relationship between *ELK3-Mid51* expression levels and patients with TNBC survival outcomes, we classified patients with TNBC in the METABRIC database into *ELK3*^{high}-*Mid51*^{low} and *ELK3*^{low}-*Mid51*^{high} groups (High, patients with TNBC with *ELK3* or *Mid51* expression in the top 15%; Low, patients with TNBC with *ELK3* or *Mid51* expression in the bottom 15%). Kaplan-Meier plots demonstrated that patients with TNBC with *ELK3*^{high}-*Mid51*^{low} expression

had significantly shorter 10-year overall survival and relapse-free survival than *ELK3*^{low}-*Mid51*^{high} patients (figure 5C). Furthermore, the immune score (representing the number of NK cells in breast tumors) indicated that *ELK3*^{low}-*Mid51*^{high} tumors had higher numbers of infiltrating NK cells than did *ELK3*^{high}-*Mid51*^{low} tumors (figure 5D). Taken together, these results demonstrate that the *ELK3-Mid51* axis is associated with responses of TNBC tumor cells to NK cells, as well as with survival outcomes.

DISCUSSION

Here, we show that *Mid51* is a direct downstream target of *ELK3*, and that the *ELK3-Mid51* axis determines the response of TNBCs to NK cells by regulating mitochondrial dynamics. Mitochondrial quality control is a dynamic flux of mitochondrial division (fission) and assembly (fusion), which allows for degradation or repair of dysfunctional elements. A qualified mitochondrial pool is necessary for all steps of TNBC development, including malignant transformation, cancer progression, migration, and resistance to chemotherapy.⁴⁷ For this reason, mitochondrial dynamics, or the genes involved in this process, have been increasingly recognized as new therapeutic targets for TNBC.⁴⁸ From this perspective, our results provide insight into the development of novel therapeutic strategies and treatment landscapes for the management of TNBC.

It has previously been reported that killer lymphocyte granzyme B induces superoxide in target cells by directly inducing mitochondrial complex-1 dysfunction, which is required for the onset of apoptosis.^{49,50} Given that cancer cells require a certain level of ROS to initiate apoptosis, mitochondrial fission-mediated ROS generation in *ELK3KD* TNBCs may have rendered these cells vulnerable to NK cells.

Combining the results of our previous report with those presented herein suggests that *ELK3* is a master regulator of two main characteristics of TNBCs: metastasis²⁷ and responses to NK cells. Although we demonstrated that *ELK3-Mid51* axis-mediated modulation of mitochondrial dynamics is linked directly to TNBC responses to NK cells, it remains to be clarified whether this axis also functions as a control tower for epithelial-mesenchymal transition (EMT) and metastasis of TNBC. According to our data, *ELK3*-suppressed TNBCs are less metastatic and more sensitive to NK cell-mediated cytotoxicity. Therefore, we do not rule out the possibility that the *ELK3-Mid51* axis is also linked to the metastatic phenotype of these cells. However, there are several contradictory reports about the immune responses of mesenchymal cancer cells. For example, EMT renders cancer cells more sensitive to NK-mediated cytotoxicity by modulating expression of activating and inhibitory ligands.⁵¹ In addition, myocardin-related transcription factors, which promote metastatic invasion of melanoma and breast cancer cells, sensitize cancer cells to cytotoxic lymphocytes by

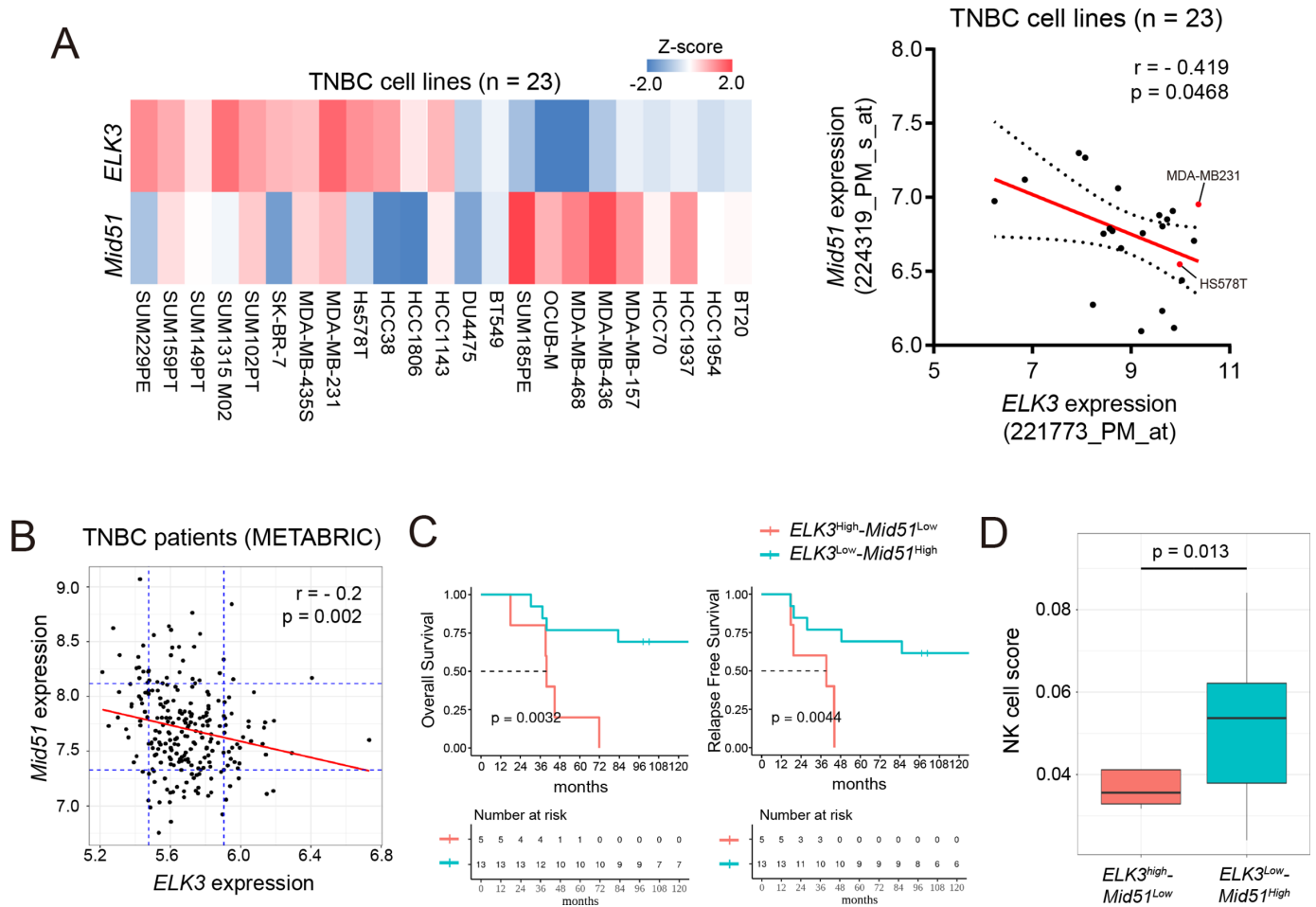


Figure 5 The ELK3-Mid51 axis plays a role in immunosurveillance by NK cells in patients with TNBC. (A) Heat map (left) and correlation graph (right) of *ELK3* and *Mid51* messenger RNA expression in 23 TNBC cell lines for which whole genome expression profiles were obtained from public microarray data sets (GSE41313). (B) Correlation between *ELK3* and *Mid51* expression levels in 236 patients with TNBC for whom whole genome expression profiles were obtained from METABRIC. (C) Kaplan-Meier analysis of overall survival and relapse-free survival of *ELK3*^{low}-*Mid51*^{high} and *ELK3*^{high}-*Mid51*^{low} patients with TNBC. Patients with TNBC with *ELK3* expression in the bottom 15% and *Mid51* expression in the top 15% were labeled as '*ELK3*^{low} and *Mid51*^{high}' (n=13), while patients with TNBC with *ELK3* expression in the top 15% and *Mid51* expression in the bottom 15% were labeled as '*ELK3*^{high} and *Mid51*^{low}' (n=5). (D) NK cell scores for *ELK3*^{low}-*Mid51*^{high} and *ELK3*^{high}-*Mid51*^{low} patients with TNBC. Statistical significance in (A) and (B) was calculated based on Pearson's correlation coefficient. The p values in (C) and the box plots (D) were calculated by the log-rank test and Welch's t-test, respectively. ELK3, transcription factor; Mid51, mitochondrial dynamics proteins of 51; NK, natural killer; TNBC, triple negative breast cancer.

increasing their rigidity.⁵² Since ELK3 KD TNBCs show epithelial cell-like morphology and fewer metastatic characteristics,²⁷ it is not clear to us how epithelial-like cancer cells showed highly sensitive responses to NK cells both in vitro and in vivo.

One possible explanation is that the ELK3-Mid51 axis links to metastasis of TNBCs by adjusting the delicate balance between mitochondrial fission and fusion in TNBCs. It is plausible that there is an optimal window of ELK3 expression, which renders TNBCs more metastatic and less immunogenic at the same time. Considering that mitochondrial fission is linked directly to increased ROS formation, we can estimate that there is an appropriate range of mitochondrial fission status and ROS levels that favor metastasis of TNBC; therefore, excessive mitochondrial fission and ROS production might make cells more

vulnerable to the various stresses that induce apoptotic cell death. This idea is supported by the fact that mitochondrial fission status is critical for determining the metastatic fate and apoptosis of TNBCs. During the early stages of TNBC development, high mitochondrial ROS levels increase metastatic potential,⁵³ whereas excessive ROS production causes cell damage and subsequent initiation of apoptosis.⁵⁴ The concept of an appropriate level or window of mitochondrial fission might be further supported by controversial reports about the role of mitochondrial dynamics in metastasis of TNBCs. For example, increased mitochondrial fission in clinical samples of TNBCs correlates with poor survival of patients with TNBC,⁵⁵ and highly metastatic hepatocellular carcinoma displays excessive mitochondrial fission.⁵⁶ By contrast, enforcing mitochondrial fission through genetic or

chemical approaches suppresses metastasis in a TNBC mouse model, and treatment with a potent chemical activator of mitochondrial fusion proteins overcomes these suppressive phenotypes.⁵⁷ The first step toward clarifying the roles of mitochondrial fission and ROS concentrations in cancer immune responses and metastasis would be to dissect existing data sets of human malignancies for data related to mitochondrial dynamics, immunogenic indices, and patient survival.

Another possibility is that ELK3-Mid51-mediated modulation of mitochondrial dynamics and subsequent susceptibility to NK cells is not linked to the metastatic phenotype of TNBCs. As a master regulator that orchestrates metastasis of TNBCs, ELK3 regulates various genes, including E-cadherin, SERPINE1, and GATA3, during the initiation and execution of EMT and metastasis.^{26 27 58}

Considering that most of these genes are not implicated in mitochondrial activity or dynamics, we cannot rule out the possibility that ELK3 has a pleiotropic function in TNBCs to regulate metastasis, mitochondrial dynamics, and immune responses simultaneously, or that the phenotype of TNBCs is the result of fine tuning of expression of ELK3 target genes. In line with this possibility, it would be interesting to see whether metastatic mesenchymal TNBCs expressing high levels of ELK3 are able to escape immunosurveillance by NK cells in patients with cancer.

The survival of patients with TNBC treated with cytotoxic chemotherapies is often compromised by the occurrence of chemoresistance and relapse of metastatic tumors.⁵⁹ Therefore, identifying effective but non-toxic therapeutic strategies is an urgent topic of TNBC research. The extreme heterogeneity of TNBC, caused by a high rate of mutations and severe genomic instability, is a serious impediment to development of chemotherapy regimens; however, paradoxically, such drawbacks make patients with TNBC suitable candidates for immunotherapy.^{60 61}

CONCLUSIONS

In conclusion, our data strongly suggest that the ELK3-Mid51 axis is a major determinant of immunosensitivity of TNBCs to NK cells. We believe that these results increase our understanding of the role of ELK3 in regulating immune evasion, as well as EMT and metastasis, of TNBCs. TNBC is the most aggressive breast cancer subtype; therefore, efficient treatment is an unmet clinical need. These data provide a promising strategy for increasing the immunotherapeutic efficacy of NK cells against these cancers.

Contributors JDP and K-SP designed the project and wrote the manuscript. JDP, K-SK, SHC, J-HC, S-WP, HJJ, ML, D-KL, and E-SK performed the experiments. GHJ and SH performed bioinformatic analysis. JDP, H-YJ, and K-SP analyzed the data and discussed the results. K-SP is responsible for the overall content as the guarantor.

Funding This work was supported by the Basic Science Research Program through the National Research Foundation of Korea (NRF), funded by the Ministry of Education (2019R1A6A1A03032888, NRF-2022R1A2C1003390).

Competing interests No, there are no competing interests.

Patient consent for publication Not applicable.

Ethics approval All animal experiments were approved by the Institutional Animal Care and Use Committee of the laboratory animal research center at CHA University (IACUC-200011). Primary natural killer cells were isolated from peripheral blood mononuclear cells obtained from healthy donors. This research was reviewed and approved by the institutional review board of CHA University (permit number: 1044308-202112-HR-097-02). All healthy blood donors provided informed consent.

Provenance and peer review Not commissioned; externally peer reviewed.

Data availability statement All data relevant to the study are included in the article or uploaded as supplementary information.

Supplemental material This content has been supplied by the author(s). It has not been vetted by BMJ Publishing Group Limited (BMJ) and may not have been peer-reviewed. Any opinions or recommendations discussed are solely those of the author(s) and are not endorsed by BMJ. BMJ disclaims all liability and responsibility arising from any reliance placed on the content. Where the content includes any translated material, BMJ does not warrant the accuracy and reliability of the translations (including but not limited to local regulations, clinical guidelines, terminology, drug names and drug dosages), and is not responsible for any error and/or omissions arising from translation and adaptation or otherwise.

Open access This is an open access article distributed in accordance with the Creative Commons Attribution Non Commercial (CC BY-NC 4.0) license, which permits others to distribute, remix, adapt, build upon this work non-commercially, and license their derivative works on different terms, provided the original work is properly cited, appropriate credit is given, any changes made indicated, and the use is non-commercial. See <http://creativecommons.org/licenses/by-nc/4.0/>.

ORCID iDs

Joo Dong Park <http://orcid.org/0000-0002-6131-878X>

Seung Hee Choi <http://orcid.org/0000-0002-8736-7969>

Kyung-Soon Park <http://orcid.org/0000-0002-0615-4313>

REFERENCES

- June CH, Sadelain M. Chimeric antigen receptor therapy. *N Engl J Med* 2018;379:64–73.
- Lorenzo-Herrero S, López-Soto A, Sordo-Bahamonde C, et al. Nk cell-based immunotherapy in cancer metastasis. *Cancers* 2018;11. doi:10.3390/cancers11010029. [Epub ahead of print: 28 12 2018].
- Gonzalez-Rodriguez AP, Villa-Álvarez M, Sordo-Bahamonde C, et al. Nk cells in the treatment of hematological malignancies. *J Clin Med* 2019;8. doi:10.3390/jcm8101557. [Epub ahead of print: 27 09 2019].
- Buchwalter G, Gross C, Wasylyk B. Ets ternary complex transcription factors. *Gene* 2004;324:1–14.
- Albertsson PA, Basse PH, Hokland M, et al. Nk cells and the tumour microenvironment: implications for NK-cell function and anti-tumour activity. *Trends Immunol* 2003;24:603–9.
- Mandal R, Şenbabaoğlu Y, Desrichard A, et al. The head and neck cancer immune landscape and its immunotherapeutic implications. *JCI Insight* 2016;1:e89829.
- Nguyen R, Wu H, Pounds S, et al. A phase II clinical trial of adoptive transfer of haploidentical natural killer cells for consolidation therapy of pediatric acute myeloid leukemia. *J Immunother Cancer* 2019;7:81.
- Rezvani K, Rouce RH. The application of natural killer cell immunotherapy for the treatment of cancer. *Front Immunol* 2015;6:578.
- Stojanovic A, Cerwenka A. Natural killer cells and solid tumors. *J Innate Immun* 2011;3:355–64.
- Nunnari J, Suomalainen A. Mitochondria: in sickness and in health. *Cell* 2012;148:1145–59.
- Detmer SA, Chan DC. Functions and dysfunctions of mitochondrial dynamics. *Nat Rev Mol Cell Biol* 2007;8:870–9.
- Jheng H-F, Tsai P-J, Guo S-M, et al. Mitochondrial fission contributes to mitochondrial dysfunction and insulin resistance in skeletal muscle. *Mol Cell Biol* 2012;32:309–19.
- Kobashigawa S, Suzuki K, Yamashita S. Ionizing radiation accelerates Drp1-dependent mitochondrial fission, which involves delayed mitochondrial reactive oxygen species production in normal human fibroblast-like cells. *Biochem Biophys Res Commun* 2011;414:795–800.
- Picard M, Shirihai OS, Gentil BJ, et al. Mitochondrial morphology transitions and functions: implications for retrograde signaling? *Am J Physiol Regul Integr Comp Physiol* 2013;304:R393–406.

- 15 Willems PHGM, Rossignol R, Dieteren CEJ, et al. Redox homeostasis and mitochondrial dynamics. *Cell Metab* 2015;22:207–18.
- 16 Pletjushkina OY, Lyamzaev KG, Popova EN, et al. Effect of oxidative stress on dynamics of mitochondrial reticulum. *Biochim Biophys Acta* 2006;1757:518–24.
- 17 Chen H, Chan DC. Emerging functions of mammalian mitochondrial fusion and fission. *Hum Mol Genet* 2005;14 Spec No. 2:R283–9.
- 18 Zhu P-P, Patterson A, Stadler J, et al. Intra- and intermolecular domain interactions of the C-terminal GTPase effector domain of the multimeric dynamin-like GTPase Drp1. *J Biol Chem* 2004;279:35967–74.
- 19 Kalia R, Wang RY-R, Yusuf A, et al. Structural basis of mitochondrial receptor binding and constriction by drp1. *Nature* 2018;558:401–5.
- 20 Zhang X, Li F, Cui Y, et al. Mst1 overexpression combined with YAP knockdown augments thyroid carcinoma apoptosis via promoting MIEF1-related mitochondrial fission and activating the JNK pathway. *Cancer Cell Int* 2019;19:143.
- 21 Romani P, Nirchio N, Arboit M, et al. Mitochondrial fission links ECM mechanotransduction to metabolic redox homeostasis and metastatic chemotherapy resistance. *Nat Cell Biol* 2022;24:168–80.
- 22 Dasgupta A, Chen K-H, Wu D, et al. An epigenetic increase in mitochondrial fission by MID49 and MID51 regulates the cell cycle in cancer: diagnostic and therapeutic implications. *Faseb J* 2020;34:5106–27.
- 23 Hou Y, Lan C, Kong Y, et al. Genetic ablation of TAZ induces HepG2 liver cancer cell apoptosis through activating the CaMKII/MIEF1 signaling pathway. *Oncotargets Ther* 2019;12:1765–79.
- 24 Giovane A, Pintzas A, Maira SM, et al. Net, a new Ets transcription factor that is activated by Ras. *Genes Dev* 1994;8:1502–13.
- 25 Zheng H, Wasyluk C, Ayadi A, et al. The transcription factor net regulates the angiogenic switch. *Genes Dev* 2003;17:2283–97.
- 26 Cho H-J, Oh N, Park J-H, et al. Zeb1 collaborates with ELK3 to repress E-cadherin expression in triple-negative breast cancer cells. *Mol Cancer Res* 2019;17:2257–66.
- 27 Kong S-Y, Kim K-S, Kim J, et al. The ELK3-GATA3 axis orchestrates invasion and metastasis of breast cancer cells in vitro and in vivo. *Oncotarget* 2016;7:65137–46.
- 28 Oh N, Park J-I, Park J-H, et al. The role of ELK3 to regulate peritumoral lymphangiogenesis and VEGF-C production in triple negative breast cancer cells. *Biochem Biophys Res Commun* 2017;484:896–902.
- 29 Yang H, Schramek D, Adam RC, et al. Ets family transcriptional regulators drive chromatin dynamics and malignancy in squamous cell carcinomas. *Life* 2015;4:e10870.
- 30 Semenchenko K, Wasyluk C, Cheung H, et al. XRP44X, an inhibitor of Ras/ERK activation of the transcription factor ELK3, inhibits tumour growth and metastasis in mice. *PLoS One* 2016;11:e0159531.
- 31 Crique-Filipe P, Ducret C, Maira SM, et al. Net, a negative ras-switchable Tcf, contains a second inhibition domain, the CID, that mediates repression through interactions with CtBP and deacetylation. *Embo J* 1999;18:3392–403.
- 32 Tsoyi K, Geldart AM, Christou H, et al. Elk-3 is a KLF4-regulated gene that modulates the phagocytosis of bacteria by macrophages. *J Leukoc Biol* 2015;97:171–80.
- 33 Kim K-S, Park K-S. XRP44X enhances the cytotoxic activity of natural killer cells by activating the c-Jun N-terminal kinase signaling pathway. *Dev Reprod* 2020;24:53–62.
- 34 Riaz M, van Jaarsveld MTM, Hollestelle A, et al. miRNA expression profiling of 51 human breast cancer cell lines reveals subtype and driver mutation-specific miRNAs. *Breast Cancer Res* 2013;15:R33.
- 35 Cerami E, Gao J, Dogrusoz U, et al. The cBio cancer genomics portal: an open platform for exploring multidimensional cancer genomics data. *Cancer Discov* 2012;2:401–4.
- 36 Therneau TM, Grambsch PM. *The cox model. In: Modeling survival data: extending the Cox model*. Springer, 2000.
- 37 Sturm G, Finotello F, Petitprez F, et al. Comprehensive evaluation of transcriptome-based cell-type quantification methods for immunology. *Bioinformatics* 2019;35:i436–45.
- 38 Nakamura T, Sato T, Endo R, et al. Sting agonist loaded lipid nanoparticles overcome anti-PD-1 resistance in melanoma lung metastasis via NK cell activation. *J Immunother Cancer* 2021;9.
- 39 Lee SJ, Kang WY, Yoon Y, et al. Natural killer (NK) cells inhibit systemic metastasis of glioblastoma cells and have therapeutic effects against glioblastomas in the brain. *BMC Cancer* 2015;15:1011.
- 40 Voskoboinik I, Smyth MJ, Trapani JA. Perforin-mediated target-cell death and immune homeostasis. *Nat Rev Immunol* 2006;6:940–52.
- 41 Sarosiek KA, Chi X, Bachman JA, et al. Bid preferentially activates bak while bim preferentially activates bax, affecting chemotherapy response. *Mol Cell* 2013;51:751–65.
- 42 Kirtonia A, Sethi G, Garg M. The multifaceted role of reactive oxygen species in tumorigenesis. *Cell Mol Life Sci* 2020;77:4459–83.
- 43 Martinvalet D. Ros signaling during granzyme B-mediated apoptosis. *Mol Cell Oncol* 2015;2:e992639.
- 44 Serasinghe MN, Wieder SY, Renault TT, et al. Mitochondrial division is requisite to ras-induced transformation and targeted by oncogenic MAPK pathway inhibitors. *Mol Cell* 2015;57:521–36.
- 45 Mishra P, Chan DC. Metabolic regulation of mitochondrial dynamics. *J Cell Biol* 2016;212:379–87.
- 46 Palmer CS, Osellame LD, Laine D, et al. Mid49 and Mid51, new components of the mitochondrial fission machinery. *EMBO Rep* 2011;12:565–73.
- 47 Porporato PE, Filigheddu N, Pedro JMB-S, et al. Mitochondrial metabolism and cancer. *Cell Res* 2018;28:265–80.
- 48 Weiner-Gorzel K, Murphy M. Mitochondrial dynamics, a new therapeutic target for triple negative breast cancer. *Biochim Biophys Acta Rev Cancer* 2021;1875:188518.
- 49 Ricci J-E, Muñoz-Pinedo C, Fitzgerald P, et al. Disruption of mitochondrial function during apoptosis is mediated by caspase cleavage of the p75 subunit of complex I of the electron transport chain. *Cell* 2004;117:773–86.
- 50 Jacquemin G, Margiotta D, Kasahara A, et al. Granzyme B-induced mitochondrial ROS are required for apoptosis. *Cell Death Differ* 2015;22:862–74.
- 51 Chockley PJ, Chen J, Chen G, et al. Epithelial-mesenchymal transition leads to NK cell-mediated metastasis-specific immunosurveillance in lung cancer. *J Clin Invest* 2018;128:1384–96.
- 52 Tello-Lafoz M, Sspan K, Sanchez EE, et al. Cytotoxic lymphocytes target characteristic biophysical vulnerabilities in cancer. *Immunity* 2021;54:e1037.
- 53 Sarmiento-Salinas FL, Delgado-Magallón A, Montes-Alvarado JB, et al. Breast cancer subtypes present a differential production of reactive oxygen species (ROS) and susceptibility to antioxidant treatment. *Front Oncol* 2019;9:480.
- 54 Ježek J, Cooper KF, Strich R. Reactive oxygen species and mitochondrial dynamics: the yin and yang of mitochondrial dysfunction and cancer progression. *Antioxidants* 2018;7. doi:10.3390/antiox7010013. [Epub ahead of print: 16 01 2018].
- 55 Chen L, Zhang J, Lyu Z, et al. Positive feedback loop between mitochondrial fission and notch signaling promotes survivin-mediated survival of TNBC cells. *Cell Death Dis* 2018;9:1050.
- 56 Zhang Z, Li T-E, Chen M, et al. MFN1-dependent alteration of mitochondrial dynamics drives hepatocellular carcinoma metastasis by glucose metabolic reprogramming. *Br J Cancer* 2020;122:209–20.
- 57 Humphries BA, Cutter AC, Buschhaus JM, et al. Enhanced mitochondrial fission suppresses signaling and metastasis in triple-negative breast cancer. *Breast Cancer Res* 2020;22:60.
- 58 Mao Y, Li W, Hua B, et al. Silencing of ELK3 induces S-M phase arrest and apoptosis and upregulates serpinE1 expression reducing migration in prostate cancer cells. *Biomed Res Int* 2020;2020:1–9.
- 59 Isakoff SJ. Triple-negative breast cancer: role of specific chemotherapy agents. *Cancer J* 2010;16:53–61.
- 60 Loi S, Michiels S, Salgado R, et al. Tumor infiltrating lymphocytes are prognostic in triple negative breast cancer and predictive for trastuzumab benefit in early breast cancer: results from the FinHER trial. *Ann Oncol* 2014;25:1544–50.
- 61 Adams S, Gray RJ, Demaria S, et al. Prognostic value of tumor-infiltrating lymphocytes in triple-negative breast cancers from two phase III randomized adjuvant breast cancer trials: ECoG 2197 and ECoG 1199. *J Clin Oncol* 2014;32:2959–66.